

# Rainy-Season Precipitation over the Sichuan Basin and Adjacent Regions in Southwestern China

TINGTING QIAN

*State Key Laboratory of Severe Weather, Chinese Academy of Meteorological Sciences, Beijing, China*

PING ZHAO

*State Key Laboratory of Severe Weather, Chinese Academy of Meteorological Sciences, Beijing, and Collaborative Innovation Center on Forecast and Evaluation of Meteorological Disasters, Nanjing University of Information Science & Technology, Nanjing, China*

FUQING ZHANG

*Department of Meteorology, The Pennsylvania State University, University Park, Pennsylvania*

XINGHUA BAO

*State Key Laboratory of Severe Weather, Chinese Academy of Meteorological Sciences, Beijing, China*

(Manuscript received 15 May 2013, in final form 4 September 2014)

## ABSTRACT

The spatial variability and diurnal propagation of mean precipitation in the summer rainy seasons (from 2003 to 2010) over the Sichuan basin (SCB) and adjacent mountainous regions are examined using high spatiotemporal resolution satellite-derived precipitation estimates. The SCB is located just east of the Tibetan Plateau (TP) and is prone to heavy precipitation that often peaks over nighttime and early morning. The large-scale environment over the SCB during the rainy season is characterized by weak low- to midtropospheric convergence in the lee of the TP and by the upper-tropospheric jet stream to the north. Under this flow configuration, the study links the unique diurnal variations in the precipitation pattern and propagation to the unique topography in this region. It is found that during the rainy season, the local diurnal precipitation maximum moves primarily downslope and southeastward, from over the TP in the daytime to SCB at night. A secondary maximum moves northeastward downslope of the Yunnan–Guizhou Plateau toward the SCB from late evening to the early morning. The movement of precipitation over the SCB and the adjacent regions is closely tied to multiple regional-scale mountain–plain solenoids because of the large contrast in terrain heights between the basin and surrounding mountain ranges.

## 1. Introduction

The Sichuan basin (SCB) in southwestern China is one of the most populous areas in the world, with more than 100 million people. It is east of the Tibetan Plateau (TP) (which has the world's highest mountain ranges), north of the Yunnan–Guizhou Plateau (YGP), west of the Wu Mountain range (WuM), and south of the Daba Mountains

(DaM). With this unique topography, the SCB region is prone to frequent, heavy rainfall events in the warm season that often trigger deadly and costly floods and landslides; examples include long-lasting heavy rainfall events during 15–26 July 2010 (14 deaths and 11 missing) and 7–12 July 2013 (31 deaths and 160 missing).

Previous studies showed that rainfall peaks over the TP and SCB usually happen in the early evening or at midnight (Yanai and Li 1994; Yu et al. 2007; Yin et al. 2009). Some studies found summer rainfalls over TP and SCB are often triggered by subsynoptic-scale cyclones near the southeastern TP (called the southwest vortex by Chinese meteorologists), troughs in the westerlies,

---

*Corresponding author address:* Ping Zhao, State Key Laboratory of Severe Weather, Chinese Academy of Meteorological Sciences, 46 Zhongguancun South St., Beijing 100081, China.  
E-mail: zhaoping@cma.gov.cn

shear lines, and fronts over East Asia (Jiao et al. 2005; Xiao and Chen 2010). Other researchers proposed that the SCB rainfalls may have directly originated from the TP (Jiang and Fan 2002; Wang et al. 2004; Yang and Tao 2005; Yang and Smith 2006; Bai et al. 2008). For example, Wang et al. (2004) noted that convection near the eastern TP often peaks in the late afternoon or in the early evening and then propagates eastward. Bai et al. (2008) also examined a link between the nocturnal rainfall over the SCB and the eastward-propagating convective system originating over the TP. Wang et al. (2005) and Johnson (2010) discussed the southeastward propagation of rainfall from the eastern TP to SCB and the northeastward propagation from YGP to SCB.

More recently, Bao et al. (2011, hereafter BZS11) explored the diurnal variations of warm-season precipitation to the east of TP over China using high-resolution satellite estimates. They showed that the mean diurnal peak of rainfall over the eastern TP begins in the afternoon and propagates eastward toward the plains. Their dynamical analysis further showed that the propagation of diurnal rainfall is associated with several thermally driven east–west mountain–plain solenoids (MPS) because of the differential heating between mountains and plains (or oceans). In the early afternoon, the upward branch of MPS appears on the highland slopes and the downward branch appears over the plains. Around midnight, however, the downward branch appears on the highland slopes and the upward branch appears over the plains. The upward branch could enhance the diurnal peak of the local precipitation. Similar propagating features of rainfall were also seen over other mountainous areas of China and the United States (Zhang and Koch 2000; Koch et al. 2001; Yang and Slingo 2001; Carbone et al. 2002; Chen et al. 2008; He and Zhang 2010; Huang et al. 2010; Trier et al. 2010).

As a follow up of BZS11, the current study focuses exclusively on the diurnal variation and propagation of warm-season precipitation over the SCB and adjacent mountain slopes in relation to the unique basin topography and large-scale flow patterns over this region. We are particularly interested in how different orientation of the terrain slopes (not purely due east–west as assumed in BZS11), along with the presence of the downstream mountain ranges, will alter the diurnal rainfall peak evolution. Averaged along straight longitude lines, the time–longitude diagram (i.e., in the zonal direction) in BZS11 suggested that the diurnal rainfall peak propagates eastward at a nearly constant velocity from the TP to the SCB and then to the plains. The current research also complements the study of He and Zhang (2010), which examined the impact of a regional MPS over north China.

In section 2, we specify the study domain, define the “rainy season” in the SCB, and describe the data and

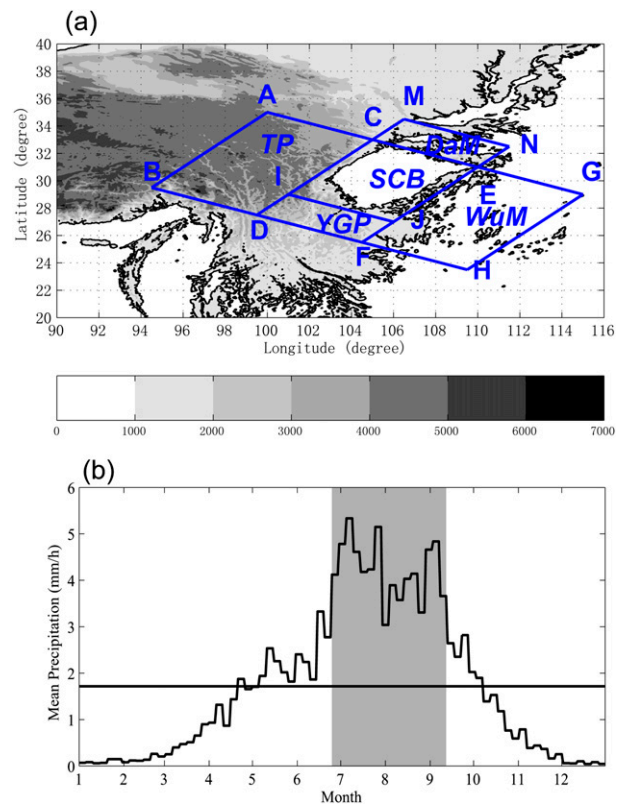


FIG. 1. (a) Terrain height highlighted in the parallelograms ABHG and DFNM, in which are the eastern TP, SCB, the WuM to the east of SCB, YGP to the south of SCB, and the DaM to the north of SCB. The black contours are for the terrain height of 1000 m. (b) Climatological (1960–2000) and regional (SCB) series of 5-day mean rainfall ( $\text{mm day}^{-1}$ ), in which the horizontal black solid line is for the annual mean value of daily rainfall. The gray shading indicates the rainy period.

methodology. Section 3 investigates the various features of diurnal rainfall in the rainy season, including propagation and diurnal variations of precipitation. The effects of large-scale environment and multiple thermally driven regional-scale MPSs on rainy-season rainfall are examined in section 4. Finally, we give a summary and a discussion in section 5.

## 2. Data and methodology

Figure 1a shows a map of southwestern China with terrain elevation shaded. Our focus regions are the parallelograms labeled ABHG and DFNM. Following Zhao et al. (2010), we define the rainy period from a climatological perspective using the daily precipitation measured by rain gauge stations during 1960–2000. Figure 1b shows the time series of the climatological 5-day (pentad) mean precipitation rate averaged over all available rain gauges within the SCB. For this domain, the annual

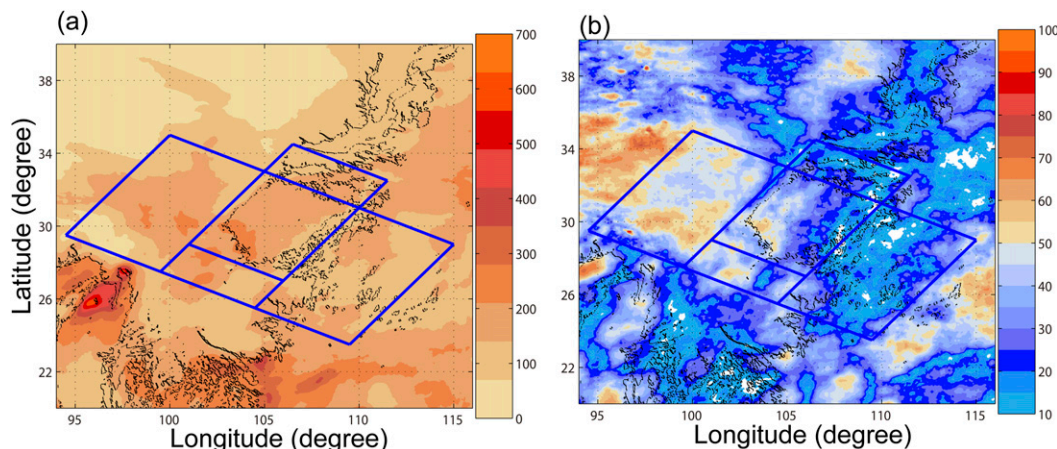


FIG. 2. (a) Distribution of mean monthly total precipitation (mm) during the rainy season. The black contours are for the terrain height of 1000 m. The region in the blue parallelograms is the focus area. (b) Percentage of the diurnal contributions of the total precipitation averaged over the rainy season (defined in BZS11).

mean rain rate is  $1.7 \text{ mm day}^{-1}$ . We define the SCB rainy period as the time span with a continuous 5-day mean rain rate above  $3 \text{ mm day}^{-1}$ , which begins on 20 June and ends on 11 September.

For the rest of the study, we will use the precipitation product with a horizontal grid spacing of approximately 8 km and a time interval of 30 min derived from several low orbit satellite microwave data via the Climate Prediction Center morphing technique (CMORPH; Joyce et al. 2004). The CMORPH precipitation estimate has been used to investigate rainfall features in China (He and Zhang 2010; Shen et al. 2010; BZS11). Their results showed that the CMORPH estimation is well suited to

examine the detailed spatial patterns and temporal variations of warm-season precipitation in China, including the SCB focus area in this study.

To better understand the large-scale flow configurations and regional-scale circulations, we also use the atmospheric temperature, geopotential height, wind, and relative humidity derived from the National Centers for Environmental Prediction (NCEP) Final (FNL) Operational Global Analysis dataset (<http://rda.ucar.edu/datasets/ds083.2>). The FNL dataset has a horizontal grid spacing of  $1^\circ \times 1^\circ$  in both longitude and latitude and includes the surface level and 26 pressure levels in the vertical. The FNL is available four times per day.

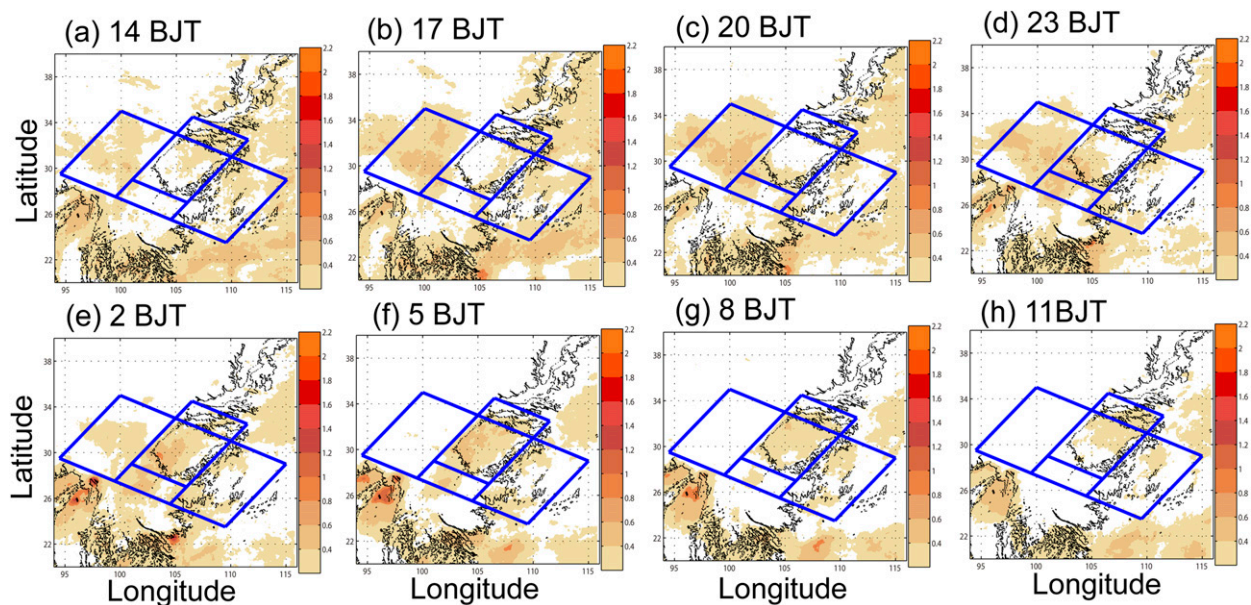


FIG. 3. Distribution of the mean rainfall in the rainy season (shading with an interval of  $0.2 \text{ mm h}^{-1}$  and greater than  $0.2 \text{ mm h}^{-1}$ ) at (a) 1400, (b) 1700, (c) 2000, (d) 2300, (e) 0200, (f) 0500, (g) 0800, and (h) 1100 BJT. The black contour is for the terrain height of 1000 m.

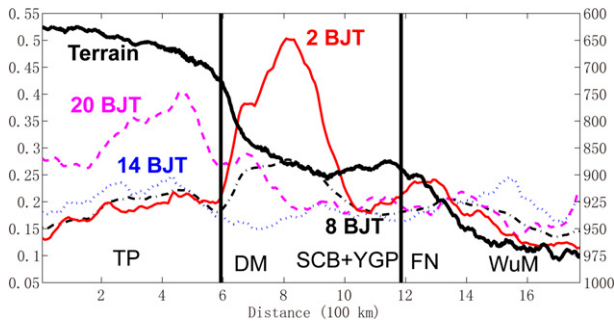


FIG. 4. The terrain elevation (black solid line) and hourly mean rainfall ( $\text{mm h}^{-1}$ ) at 1400 (blue dotted line), 2000 (violet dashed line), 0200 (red solid line), and 0800 BJT (black dashed-dotted line) along the northwest-southeast (parallel line BH) direction averaged over the boxed focus area ABHG in the rainy season. Vertical thick lines are for the lines DM (left) and FM (right).

The 8-yr (2003–10) mean values are used to examine the diurnal variations of rainfall, the large-scale environment, and the basinwide atmospheric circulation over the focus region. To better represent the effect of terrain on the SCB precipitation (and its diurnal variation), the skewed coordinates with cross sections averaged directly perpendicular to terrain slopes are applied following Ahijevych et al. (2004) and He and Zhang (2010). The cross section along line BH (Fig. 1a) is obtained from the skewed coordinates within the parallelogram ABHG with the average direction parallel line CD.

### 3. Diurnal characteristics of precipitation

Figure 2a shows the spatial distribution of monthly-mean total precipitation (from 2003 to 2010) over the SCB and surrounding areas during the rainy season, as

derived from the CMORPH dataset. The monthly-mean rainfall over nearly the entire basin is greater than  $140 \text{ mm}$ , with the highest amounts of over  $200 \text{ mm month}^{-1}$  located at the southwest corner (on the immediate leeside/northeast of YGP as well as to lee of TP) and the lowest amounts on the southeast side of the basin. Monthly precipitation amounts over most of the lee slopes of TP and the northwest part of the YGP lee slopes exceed  $140 \text{ mm}$ , with values greater than  $210 \text{ mm}$  in some localized areas on both terrain slopes.

Figure 2b shows the percentage of the diurnal contributions of the total precipitation averaged over the rainy season following the calculation described in BZS11 and He and Zhang (2010). The diurnal percentage (DP) is defined in BZS11 as

$$DP = \frac{\sum_{t=1}^{24} |r_t - \bar{r}|}{r_d}, \quad (1)$$

where  $r_t$  is the mean rainfall rate at each hour,  $\bar{r}$  is the mean hourly precipitation rate, and  $r_d$  is the mean daily precipitation. The importance of diurnal variation of daily precipitation over the focus region (the primary objective of this study) becomes clear: nearly 50% of the total precipitation over the southwestern two-thirds of the SCB during the rainy period comes from the diurnal contributions, with even higher percentages over most of the lee slopes of TP and YGP. The diurnal contribution decreases rapidly toward the upstream slopes of the Wu and Daba Mountain ranges.

Figure 3 shows the averaged diurnal cycle of the rainy-season precipitation over the SCB and the surrounding region, every 3 h starting at 1400 Beijing time (BJT), 8 h

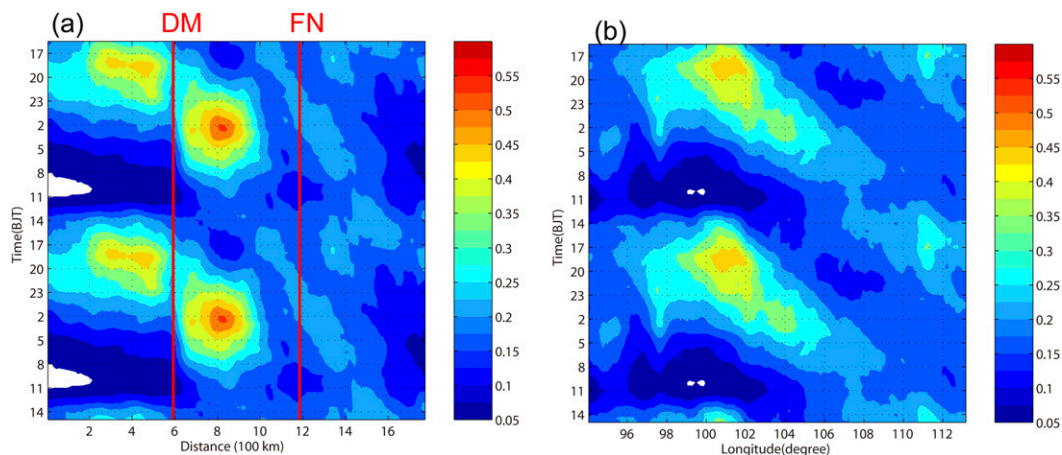


FIG. 5. The time-distance Hovmöller diagram of the rainy-season mean rainfall ( $\text{mm h}^{-1}$ ), where the cycle is repeated twice for the clarity. (a) Along the northwest-southeast (parallel line BH) direction averaged over the boxed focus area ABHG. Vertical thick lines are for the lines (left) DM and (right) FM. (b) Along the cross section with the average between the latitudes  $27^{\circ}$ – $35^{\circ}\text{N}$ .

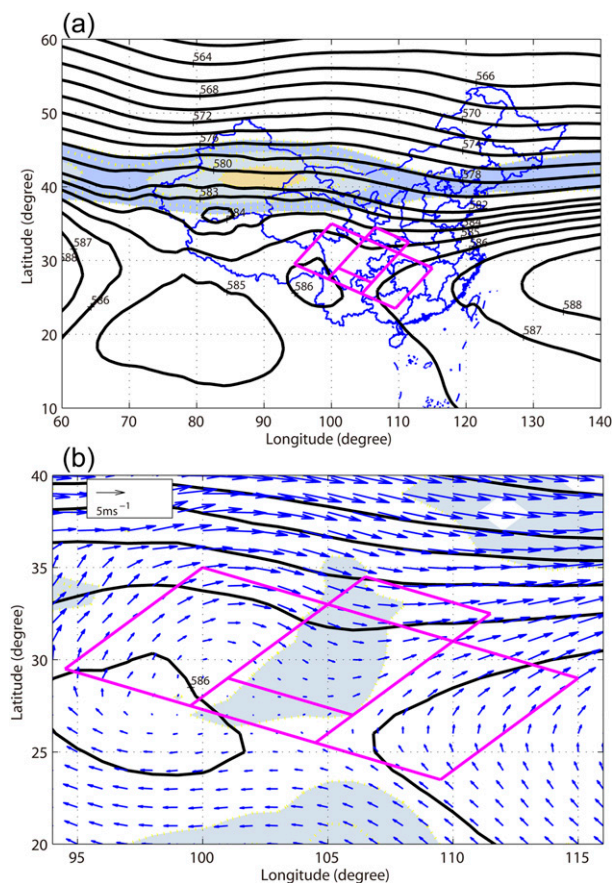


FIG. 6. (a) Mean 500-hPa geopotential height (contour interval = 1 at the low latitude and 2 at the high latitude; units are gpm) and 200-hPa upper-level jet greater than  $26 \text{ m s}^{-1}$  (shaded region; contour interval =  $2 \text{ m s}^{-1}$ ; maximum wind speed =  $35.1 \text{ m s}^{-1}$ ) in rainy period. The blue contour is country map. The violet parallelograms are the focus area. (b) Mean 500-hPa geopotential height (contours), 700-hPa positive relative vorticity (shaded) in the study region, and 500-hPa horizontal wind (vectors).

ahead of UTC). The local diurnal rainfall maximum first develops on the eastern slope of the TP just east of  $100^\circ\text{E}$  before the local noontime (2 h behind BJT); some residual diurnal precipitation from the previous day is located in the northeastern half of the SCB (Fig. 3a). In the early afternoon the diurnal precipitation on the eastern slope of the TP expands in areal coverage and intensifies, with the line of peak precipitation shifting to a northeast–southwestward orientation and sliding downslope toward the western edge of the SCB (Fig. 3b). Meanwhile, a weak, short-lived secondary diurnal precipitation peak develops on the southeast side of the SCB, indicative of a possible upslope rainfall initiation that is independent of the primary diurnal peak (which initiates downslope of the TP).

The primary diurnal precipitation peak from the eastern slope of the TP begins to reach the western

corner of the SCB at around 2000 BJT, at which time yet another quasi-independent secondary rainfall maximum develops, this one moving downslope of the YGP onto the southwestern side of the SCB (Fig. 3c). These two diurnal precipitation maxima merge in the late evening (2300 BJT; Fig. 3d) and cover the western half of the SCB. After midnight and through the early morning hours, the diurnal precipitation prevails throughout the entire SCB area, while diminishing first at the TP slope and then the YGP slope (Figs. 3e–g). Finally, by late morning, the diurnal precipitation weakens and retreats to the northeastern half of the SCB (Fig. 3h).

One unique finding from the above analysis is that the diurnal rainfall moves southeastward from the eastern TP to SCB in the afternoon, but does not continue to propagate southeastward or eastward across the SCB at night. This can be seen in Fig. 2a in terms of the decrease of total rainfall to the east of SCB, in Fig. 2b in terms of the diurnal contribution percentage, and in Fig. 3 in terms of the temporal evolution of the diurnal peak map distribution.

Figure 4 shows the composite analysis averaged along the upstream terrain slopes over the boxed focus area ABHG (from TP to SCB in Fig. 1). In this composite, the diurnal peak persists at nearly the same location (on the eastern edge of TP) from 1400 to 2000 BJT but shifts to persist near the center of the basin from 0200 to 0800 BJT. This rather discontinuous diurnal peak evolution can be more clearly seen in Fig. 5a, which shows the composite time–distance Hovmöller diagram of the rainy-season mean rainfall along this terrain slope. Notably, there are two distinct discontinuities on this slope: one with only a weak signal of the diurnal peak precipitation transitioning southeastward down of the TP slope (near 600 km) in the late evening, and the other nearly abrupt termination of the southeastward propagation on the east side of the SCB (near 1000 km; which is also shown in Fig. 3 discussed above).

These discontinuities are a unique finding of the current study that focuses on the local evolution of the diurnal peak precipitation in the SCB and surrounding areas through averages along a skewed coordinate, in comparison to BZS11, that only examined the composite averaged along the zonal (east–west) direction. To directly compare with BZS11, we reproduce the composite time–distance Hovmöller diagram of the rainy-season mean rainfall averaged between the latitudes  $27^\circ$  and  $35^\circ\text{N}$  in Fig. 5b, which shows a rather continuous eastward propagation of the diurnal precipitation peaks to the east of the TP. It is evident that such latitude-averaged diurnal rainfall composite does not represent the true northeastward progression of the diurnal rainfall over this region; the skewed coordinate adopted

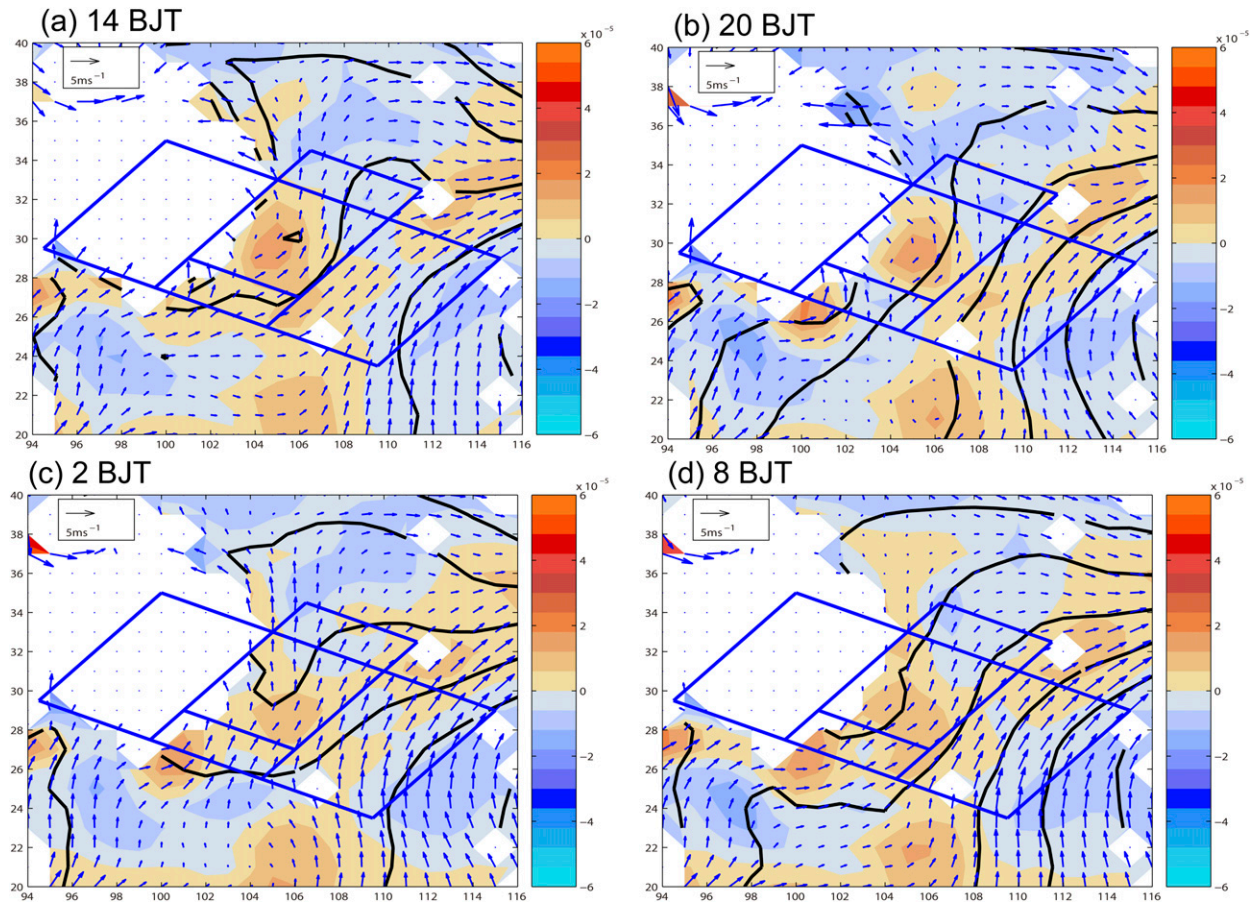


FIG. 7. Geopotential height (solid line; contour interval = 0.5 gpm), horizontal wind (vector), and vorticity (shaded) at 700 hPa at (a) 1400, (b) 2000, (c) 0200, and (d) 0800 BJT.

here (Fig. 5a), in contrast, is better at capturing the discontinuities associated with topography.<sup>1</sup>

Nevertheless, the comparison between the two composites suggests that the forcing for heaviest precipitation shifts to the lee side at night (Fig. 5a), but the large-scale midtropospheric steering flow may also have a significant contribution to the observed eastward propagation in Fig. 5b, as discussed below (see Fig. 6).

#### 4. Dynamic structures and topographic effects for diurnal rainfall

In this section, we analyze the large-scale environment and local atmospheric circulations associated with the unique diurnal variation of precipitation over the SCB and surrounding areas.

<sup>1</sup>Note that the above two different averages cover different regions, but both of them include the rainfall area of interest. Since both averages of rainfall do not include other precipitation outside the focus area, the difference in areas shall not affect the comparison.

##### a. Large-scale environment

Figure 6a shows the mean 500-hPa geopotential height and 200-hPa jet stream winds that represent the continental-scale synoptic environment during the SCB rainy season. The rainfall of interest occurs near a saddle point between the strong western Pacific subtropical high to the east, a weak South Asia subtropical high to the west, with a shallow trough in the midlatitude westerlies on the southern edge of the upper-tropospheric jet stream. In the zoom-in map plot of Fig. 6b, the SCB is mostly within the leeside convergence zone of the TP with rather persistent positive relative vorticity in the low to midtroposphere.

Figure 7 shows the diurnal variation of the mean geopotential height and relative vorticity at 700 hPa, represented by all four times available from the FNL analysis. Although it is no apparent closed vortex in the 700-hPa geopotential height or wind fields (except for maybe at 1400 BJT), a localized vorticity maximum persists over the SCB throughout the day, a signature of the commonly known southwest low vortex in China that is often found

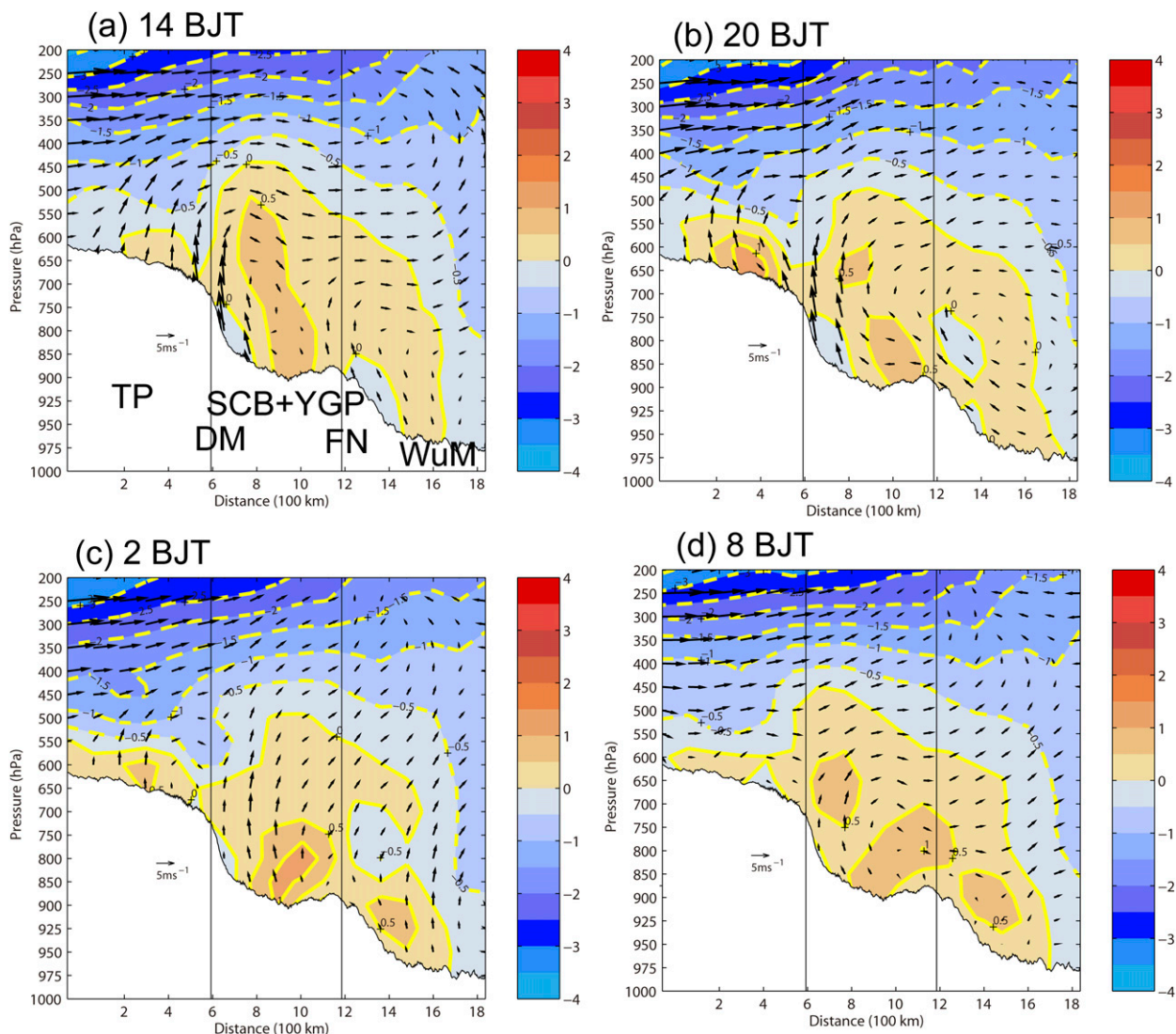


FIG. 8. The vertical cross section of the rainy-season mean vorticity (shaded;  $10^{-5} s^{-1}$ ) and vertical circulation (vectors; zonal wind in  $m s^{-1}$ ; vertical velocity in  $m s^{-1}$  multiplied by 500) along the northwest–southeast (parallel line BH) direction averaged over the boxed focus area ABHG at (a) 1400, (b) 2000, (c) 0200, and (d) 0800 BJT.

to be an efficient rain producer in this region (Huang 1986; He 2012). Associated with the shallow low-tropospheric vortex, the 700-hPa winds over the SCB are mainly from the southwest, which may bring moist air from the Bay of Bengal across the YGP into the SCB. The large-scale environment provides a favorable environment for rainy-season precipitation.

Figure 7 also shows a considerable diurnal variation in the 700-hPa vorticity field over the SCB, with the strongest positive values occurring at 1400 BJT (even with a hint of a closed geopotential low; Fig. 7a) followed by 2000 BJT (Fig. 7b). The smallest vorticity values occur at 0200 BJT (Fig. 7c) followed by 0800 BJT (Fig. 7d), at which times the low-level southwesterly flow is relatively stronger with

a farther northeastward extent; this may have contributed to the enhanced diurnal precipitation over nighttime and early morning over the SCB.

*b. Diurnal variation of MPS*

Figure 8 shows the vertical circulation and relative vorticity along the northwest–southeast (parallel line BH) direction averaged over the boxed focus area ABHG from TP to SCB; Fig. 9 shows the water vapor flux and moisture convergence (divergence) at the surface for the corresponding time. At 1400 BJT, the strong upward motion over the edges of TP—that is, the upward branch of the MPS circulation between TP and SCB (Fig. 8a)—along with surface moisture convergence (Fig. 9a) may

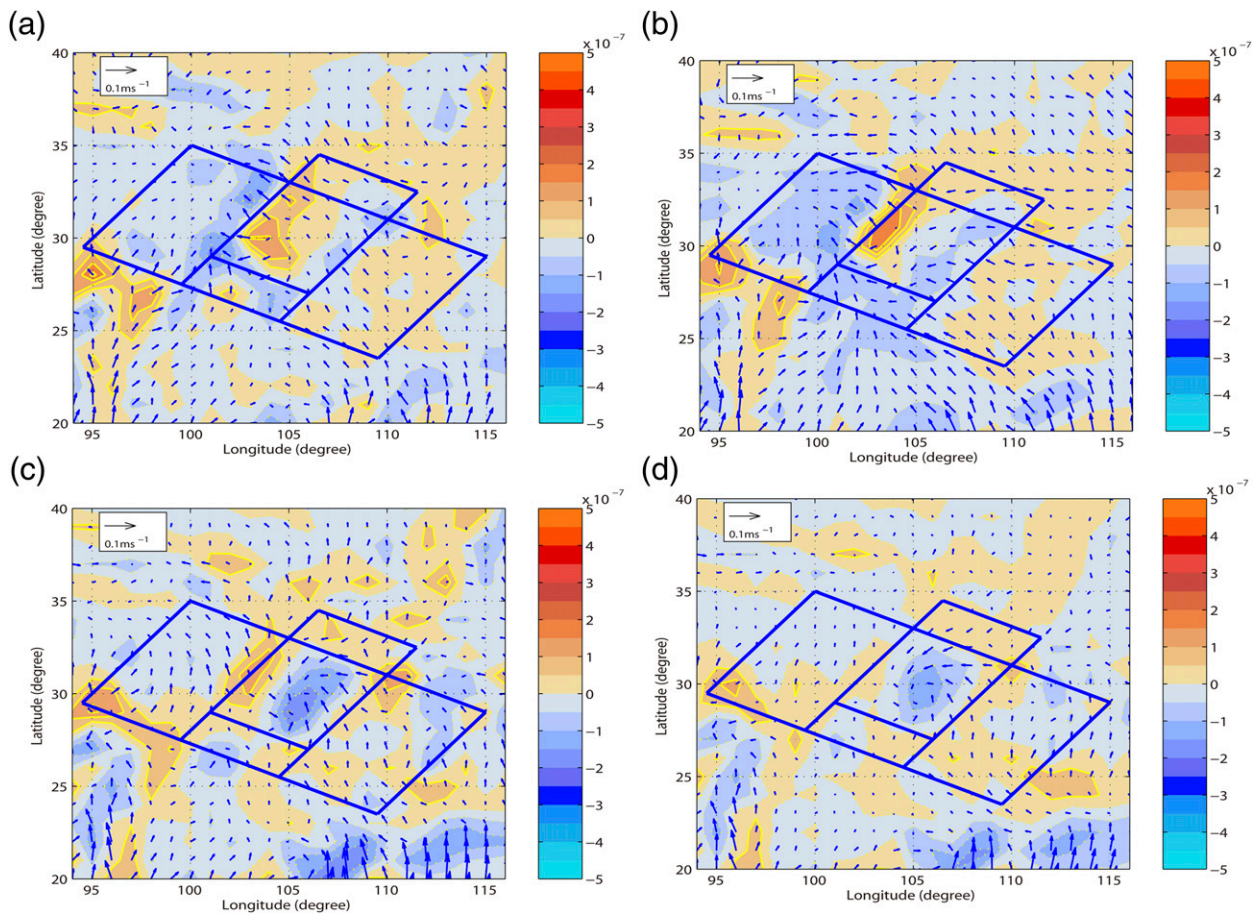


FIG. 9. Water vapor flux (vectors;  $0.1 \text{ m s}^{-1}$ ) at the surface and its convergence (contour interval =  $1 \times 10^{-7} \text{ s}^{-1}$ ; divergence is warm shading and solid lines; convergence is cold shading and dashed lines) at (a) 1400, (b) 2000, (c) 0200, and (d) 0800 BJT.

have contributed to the diurnal peak rainfall at the slope of the TP around noontime (Fig. 3a); meanwhile, prevailing downward motion suppresses rainfall over the SCB. At 2000 BJT, the rising motion spans from TP to SCB and YGP (Fig. 8b), while the surface moisture convergence only dominates TP and YGP (Fig. 9b). The southeastward spread of rising motion favors the onset of rainfall over the YGP (Fig. 3c). At 0200 BJT, the upward motion over SCB and TP (Fig. 8c) with the moisture convergence over SCB (Fig. 9c) corresponds to reduced rainfall over TP and enhanced rainfall over SCB (Fig. 3e). At 0800 BJT, both the upward motion (Fig. 8d) and the moisture convergence (Fig. 9d) are over SCB but decreasing in intensity. The weak sinking motion and moisture divergence prevailing over most of the rest of the cross section may be responsible for the discontinuity of southeastward propagation of rainfall discussed in the previous section.

To further show the diurnal variation of the MPS and its potential impact on the diurnal rainfall variations, we examine the mean 6-h changes of the vertical circulation throughout the diurnal cycle. Figure 10a (1400 minus

0800 BJT) shows two clockwise vertical circulations (i.e., the circulation tendencies are clockwise in this 6-h interval) along cross section BH within the boxed area ABHG. The left (west) circulation implies an enhanced upward branch to the west of the TP slope and an enhanced downward branch in most of the SCB. Comparing with Figs. 8a and 8d, the strengthened upward motion over the TP coincides with the occurrence of the local rainfall maximum. Another clockwise vertical circulation difference is between the SCB and its eastern region. From 1400 to 2000 BJT (Fig. 10b, cf. Figs. 8a,b), two clockwise vertical circulation differences appear over and to the east (right) of the TP. The upward branch weakens over the eastern TP, corresponding to a decrease of the local rainfall; meanwhile, the upward motion strengthens near the foothills of the eastern TP slope, accompanying the occurrence of the SCB rainfall. From 2000 to 0200 BJT (Fig. 10c, cf. Figs. 8b,c), upward motion weakens to the west (left) of the eastern TP slope, accelerating the dissipation of the local rainfall, while the increasing of upward motion appears over the

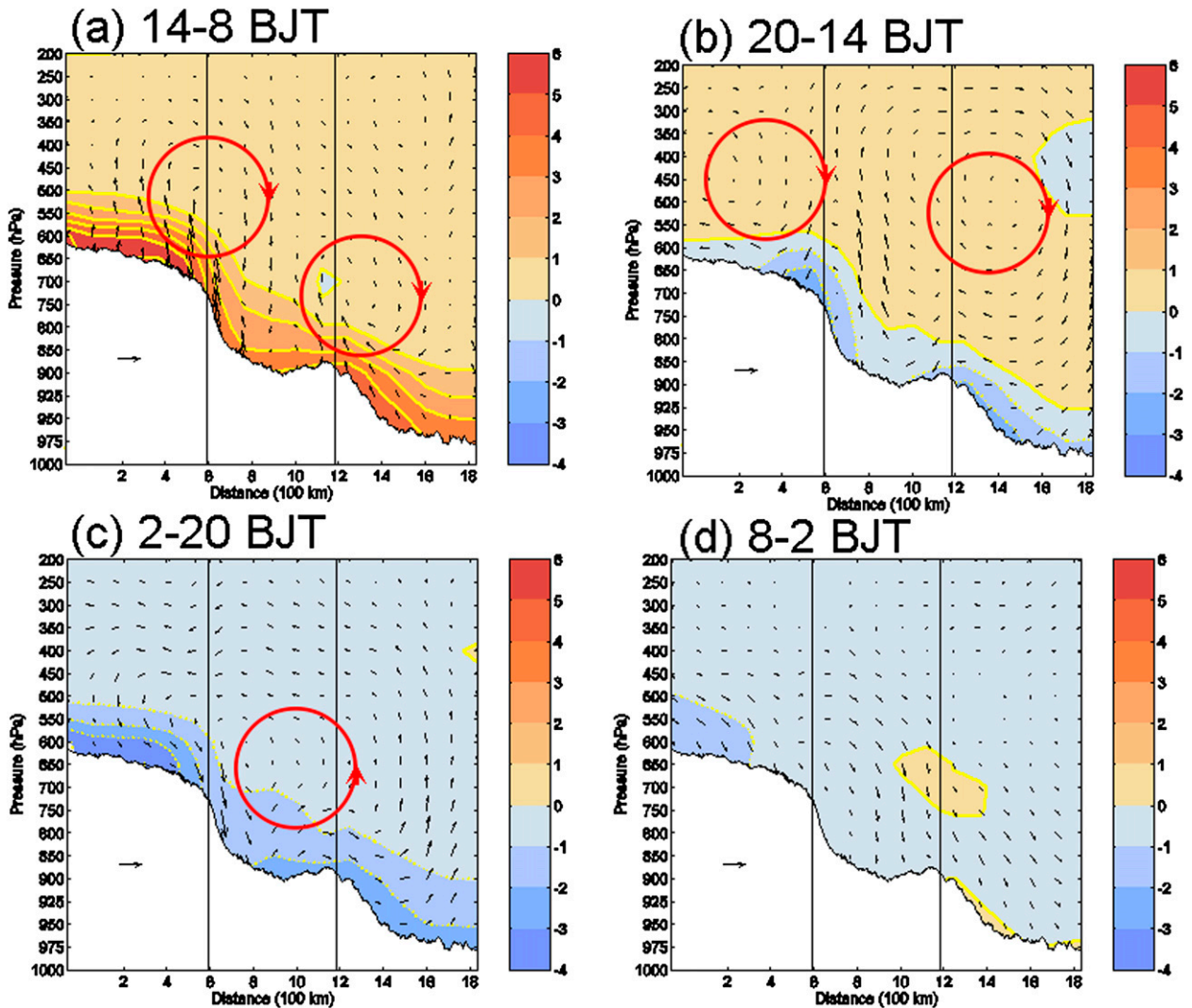


FIG. 10. The vertical circulation (vectors) and temperature difference (contour interval = 1 K; positive is warm shading and solid lines; negative is cold shading and dashed lines) along the northwest–southeast (parallel line BH) direction averaged over the boxed focus area ABHG between two times. (a) 1400 minus 0800 BJT, (b) 2000 minus 1400 BJT, (c) 0200 minus 2000 BJT, and (d) 0800 minus 0200 BJT. The reference vector shown in the lower left of each panel is  $5 \text{ ms}^{-1}$ .

SCB, providing a favorable condition for the occurrence of rainfall at night. From 0200 to 0800 BJT (Fig. 10d, cf. Figs. 8c,d), strengthening of the downward motion and weakening of the upward motion dominate the entire focus region, corresponding to the dissipation of rainfall in this period. It is evident that the diurnal and spatial variations of rainfall are closely associated with the diurnal variations of the basinwide vertical circulation.

Figure 11 shows the vertical circulation and relative vorticity along the skewed coordinate parallel line FN within the area DFNM (including SCB, YGP, and DaM). There is an anticlockwise vertical circulation above SCB and YGP at all four times. Both regions are dominated by the upward branch from 1400 to 0200 BJT,

which favors the occurrence of rainfall. Different from the primary diurnal MPS along the skewed coordinate in Fig. 8, the diurnal variation of this secondary MPS circulation in Fig. 11 is much smaller. This is likely due to a stronger influence of the dynamic effect (as flow passes topography) than the pure thermodynamic effect (induced by diurnal variations in surface heating).

The foregoing analysis shows that the dominant MPS from the northwest is due to the prevailing westerly wind past the TP in the midtroposphere (Fig. 6). There is also a secondary MPS from the southwest that is due to the prevailing southwesterly wind in the low- to mid-troposphere (Fig. 7). Meanwhile, there is no apparent upwind (and downslope) propagation of the diurnal peaks toward the SCB from the north and the east.

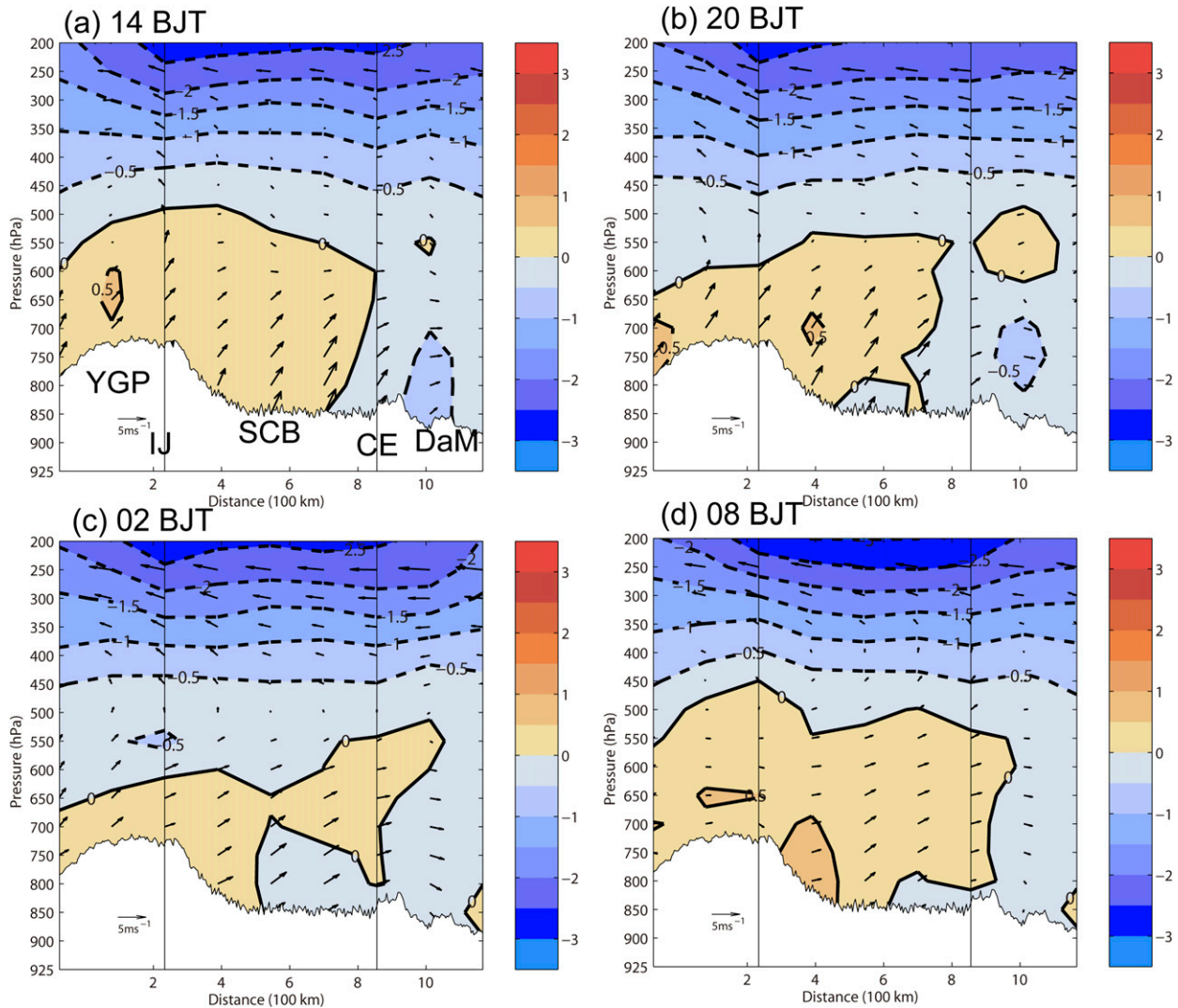


FIG. 11. As in Fig. 8, but along the skewed coordinate parallel line FN averaged over the focus region DFNM at (a) 1400, (b) 2000, (c) 0200, and (d) 0800 BJT.

### c. Possible link between temperature and MPS

Figure 10 also shows the 6-h changes in temperature along the cross section BH within the boxed area ABHG. Most of the temperature variation occurs in the terrain-following lower troposphere. In Fig. 10a, positive temperature differences between 0800 and 1400 BJT are larger over the TP and smaller over the SCB. This temperature difference favors the strengthening of a clockwise MPS circulation between TP and SCB (Fig. 10a). The temperature difference between 1400 and 2000 BJT (Fig. 10b) indicates a colder temperature variation near the surface of TP than the leeside at a similar height (below 600 hPa) from 1400 to 2000 BJT and generally corresponds to a strengthened low-tropospheric upward (downward) motion over the SCB (eastern TP) during this time (Fig. 10b).

Between 2000 and 0200 BJT, there is a larger decrease of temperature near the surface of TP than the leeside above SCB at the same height from 2000 to 0200 BJT. The different decrease in temperature changes over the eastern TP and SCB corresponds to a strengthened sinking motion over the eastern TP and ascending motion over SCB from 2000 to 0200 (Fig. 10c). Between 0200 and 0800 BJT, the temperature difference is generally weaker, with negative values below 0.5 K (Fig. 10d). It implies a weaker effect of the temperature gradient between the eastern TP and SCB on the MPS circulation.

## 5. Summary and discussion

In the present study, we document the unique diurnal evolution of rainy-season rainfall in the Sichuan basin

(SCB) as influenced by basin terrain. The results show that rainfall over the eastern TP (YGP) begins in the early afternoon (late evening) and moves southeastward (northeastward) into the SCB, but does not continue to propagate southeastward or eastward across the SCB at night. Rainfall over the SCB propagates northeastward in the early night and decays in the morning.

A dynamic analysis shows that the diurnal variation of rainfall and its eastward propagation are strongly tied to multiple MPS circulations caused by the unique basin terrain. The dominant MPS from the northwest is responsible for the southeastward propagation of precipitation between the TP and the SCB. The second MPS from the southwest accounts for the northeastward propagation of rainfall between the YGP and the SCB. The directions of these MPS circulations are tied to the 500-hPa (700 hPa) prevailing winds past the TP (YGP). The diurnal variations of the MPS are related to differential heating near the surface.

In this study, we only describe some general features of diurnal rainfall over the SCB in the rainy season and its links with the diurnal variation of rainfall over the eastern TP using several analysis and reanalysis datasets. Because the NCEP reanalysis dataset is only available at an interval of 6 h, it cannot provide sufficient information to explain the diurnal features of atmospheric conditions. Therefore, datasets with a higher temporal resolution are needed to further understand the roles of dynamic and thermodynamic effects between the SCB and adjacent regions on diurnal variations of the atmospheric circulation and rainfall. This should be addressed in future work. Moreover, using the reanalysis dataset, we do not completely separate the single effect of topography with uniform surface heating from the complex effects of topographic dynamic and thermal functions. Future investigations will use model simulations to better understand these effects.

*Acknowledgments.* We thank the anonymous reviewers, as well as Zhiyong Meng and Benjamin Green, for their valuable comments. This study is jointly sponsored by the Basic Research Fund of the Chinese Academy of Meteorological Sciences Grant 2010Y002, NSFC ATM-41105043, NSFC ATM-41221064, NSFC ATM-41175080, and U.S. NSF Grant AGS-1114849.

#### REFERENCES

- Ahijevych, D. A., C. A. Davis, R. E. Carbone, and J. D. Tuttle, 2004: Initiation of precipitation episodes relative to elevated terrain. *J. Atmos. Sci.*, **61**, 2763–2769, doi:10.1175/JAS3307.1.
- Bai, A., C. Liu, and X. Liu, 2008: Diurnal variation of summer rainfall over the Tibetan Plateau and its neighboring regions revealed by TRMM multi-satellite precipitation analysis. *Chin. J. Geophys.*, **51**, 518–529, doi:10.1002/cjg2.1242.
- Bao, X., F. Zhang, and J. Sun, 2011: Diurnal variations of warm-season precipitation east of the Tibetan Plateau over China. *Mon. Wea. Rev.*, **139**, 2790–2810, doi:10.1175/MWR-D-11-00006.1.
- Carbone, R. E., J. D. Tuttle, D. A. Ahijevych, and S. B. Trier, 2002: Inferences of predictability associated with warm season precipitation episodes. *J. Atmos. Sci.*, **59**, 2033–2056, doi:10.1175/1520-0469(2002)059<2033:IOPAWW>2.0.CO;2.
- Chen, Y., C. Wang, and Y. Li, 2008: Analysis of a heavy rain process in Sichuan basin (in Chinese). *Torrential Rain Disasters*, **27**, 301–306.
- He, G., 2012: Review of the southwest vortex research (in Chinese). *Meteor. Monogr.*, **38**, 155–163.
- He, H., and F. Zhang, 2010: Diurnal variations of warm-season precipitation over northern China. *Mon. Wea. Rev.*, **138**, 1017–1025, doi:10.1175/2010MWR3356.1.
- Huang, F., 1986: A composite analysis of the southwest vortex (in Chinese). *Sci. Atmos. Sin.*, **10**, 402–408.
- Huang, H., C. Wang, G. Chen, and R. E. Carbone, 2010: The role of diurnal solenoidal circulation on propagating rainfall episodes near the eastern Tibetan Plateau. *Mon. Wea. Rev.*, **138**, 2975–2989, doi:10.1175/2010MWR3225.1.
- Jiang, J., and M. Fan, 2002: Convective clouds and mesoscale convective systems over the Tibetan Plateau in summer (in Chinese). *Chin. J. Atmos. Sci.*, **26**, 263–270.
- Jiao, M., C. Li, and Y. Li, 2005: Mesoscale analyses of a Sichuan heavy rainfall (in Chinese). *J. Appl. Meteor. Sci.*, **16**, 699–704.
- Johnson, R. H., 2010: Diurnal cycle of monsoon convection. *The Global Monsoon System: Research and Forecast*, 2nd ed. C.-P. Chang, Ed., World Scientific Publication, 257–276.
- Joyce, R. J., J. E. Janowiak, P. A. Arkin, and P. Xie, 2004: CMORPH: A method that produces global precipitation estimates from passive microwave and infrared data at high spatial and temporal resolution. *J. Hydrometeorol.*, **5**, 487–503, doi:10.1175/1525-7541(2004)005<0487:CAMTPG>2.0.CO;2.
- Koch, S. E., F. Zhang, M. L. Kaplan, Y.-L. Lin, R. Weglarz, and C. M. Trexler, 2001: Numerical simulations of a gravity wave event over CCOPE. Part III: The role of a mountain–plains solenoid in the generation of the second wave episode. *Mon. Wea. Rev.*, **129**, 909–933, doi:10.1175/1520-0493(2001)129<0909:NSOAGW>2.0.CO;2.
- Shen, Y., A. Xiong, Y. Wang, and P. Xie, 2010: Performance of high-resolution satellite precipitation products over China. *J. Geophys. Res.*, **115**, D02114, doi:10.1029/2009JD012097.
- Trier, S. B., C. A. Davis, and D. A. Ahijevych, 2010: Environmental controls on the simulated diurnal cycle of warm-season precipitation in the continental United States. *J. Atmos. Sci.*, **67**, 1066–1090, doi:10.1175/2009JAS3247.1.
- Wang, C., G. T. Chen, and R. E. Carbone, 2004: A climatology of warm-season cloud patterns over east Asia based on GMS infrared brightness temperature observations. *Mon. Wea. Rev.*, **132**, 1606–1629, doi:10.1175/1520-0493(2004)132<1606:ACOWCP>2.0.CO;2.
- , —, and —, 2005: Variability of warm-season cloud episodes over East Asia based on GMS infrared brightness temperature observations. *Mon. Wea. Rev.*, **133**, 1478–1500, doi:10.1175/MWR2928.1.
- Xiao, H., and J. Chen, 2010: Numerical study of one plateau vortex moving eastward affecting heavy rainfall in Sichuan (in Chinese). *Plateau Mt. Meteor. Res.*, **30**, 12–17.
- Yanai, M., and C. Li, 1994: Mechanism of heating and the boundary layer over the Tibetan Plateau. *Mon. Wea. Rev.*, **122**, 305–323, doi:10.1175/1520-0493(1994)122<0305:MOHATB>2.0.CO;2.

- Yang, B., and Z. Tao, 2005: The analysis of local features of MCC on southeast Tibetan Plateau (in Chinese). *Acta Meteor. Sin.*, **63**, 236–242.
- Yang, G., and J. Slingo, 2001: The diurnal cycle in the tropics. *Mon. Wea. Rev.*, **129**, 784–801, doi:10.1175/1520-0493(2001)129<0784:TDCITT>2.0.CO;2.
- Yang, S., and E. A. Smith, 2006: Mechanisms for diurnal variability of global tropical rainfall observed from TRMM. *J. Climate*, **19**, 5190–5226, doi:10.1175/JCLI3883.1.
- Yin, S., D. Chen, and Y. Xie, 2009: Diurnal variations of precipitation during the warm season over China. *Int. J. Climatol.*, **29**, 1154–1170, doi:10.1002/joc.1758.
- Yu, R., T. Zhou, A. Xiong, Y. Zhu, and J. Li, 2007: Diurnal variations of summer precipitation over contiguous China. *Geophys. Res. Lett.*, **34**, L01704, doi:10.1029/2006GL028129.
- Zhang, F., and S. E. Koch, 2000: Numerical simulations of a gravity wave event over CCOPE. Part II: Waves generated by an orographic density current. *Mon. Wea. Rev.*, **128**, 2777–2796, doi:10.1175/1520-0493(2000)128<2777:NSOAGW>2.0.CO;2.
- Zhao, P., S. Yang, and R. Yu, 2010: Long-term changes in rainfall over eastern China and large-scale atmospheric circulation associated with recent global warming. *J. Climate*, **23**, 1544–1562, doi:10.1175/2009JCLI2660.1.